Ceramics International 49 (2023) 10852–10863

Contents lists available at ScienceDirect

Ceramics International

journal homepage: www.elsevier.com/locate/ceramint

Unusual crystallization pathways revealed in six barium disilicate ($BaSi_2O_5$) glasses

Benjamin J.A. Moulton [a,b,c,*], Laís D. Silva [b], Simone R.F. Sabino [d], Leonardo L. Evaristo [e], David V. Sampaio [f], Silvio Buchner [e], Francisco C. Serbena [d], Paulo S. Pizani [a,b], Edgar D. Zanotto [b]

[a] Universidade Federal de São Carlos, Departamento de Física, Rod. Washington Luis, Km 235 13565-905, São Carlos, SP, Brazil
[b] CERTEV — Center for Research, Technology, and Education in Vitreous Materials, Department of Materials Engineering, Federal University of São Carlos, 13565 - 905, São Carlos, SP, Brazil
[c] Friedrich-Alexander-Universität Erlangen-Nürnberg, Institute of Glass and Ceramics, Martensstraße 5, 91058, Erlangen, Germany
[d] Department of Physics, State University of Ponta Grossa (UEPG), Ponta Grossa, PR, 84030-900, Brazil
[e] Institute of Physics, Federal University of Rio Grande do Sul, Porto Alegre, RS, 91501-970, Brazil
[f] Institute of Physics, Federal University of Alagoas, 57072-970, Maceió, AL, Brazil

ARTICLE INFO

Keywords:
Homogeneous nucleation
Barium disilicate $BaSi_2O_5$ glass
Sanbornite
$Ba_6Si_{10}O_{26}$
$Ba_5Si_8O_{21}$
Raman spectroscopy
X-ray diffraction
DSC calorimetry
Silicate liquid

ABSTRACT

Due to the unusual crystallization of (nominally) stoichiometric $BaSi_2O_5$ (BS2) glass, which shows unexpected and diverse crystal phases, a series of six glasses with different chemicals and melting procedures were prepared in three laboratories and characterized before and after crystallization by differential scanning calorimetry, density measurements, X-ray diffraction, FTIR, and Raman spectroscopy. The aim of this study was to assess whether there is systematic behavior in the crystallization pathways in relation to precursor chemicals, impurities, and hydroxyl content of this glass. Small glass monoliths were treated at the first DSC crystallization peak and quenched to determine which phases formed in the early-stages of crystallization. The glass transition temperatures (T_g) divide these six glasses between those with a T_g near 690 °C versus those near 700 °C. The DSC peak crystallization temperatures varied even more; from 855 to 917 °C. In these six glasses, our results are best explained by a combination of metastable high-$BaSi_2O_5$ and $Ba_6Si_{10}O_{26}$. Monotonic trends in crystallization show that the DSC signal from the Ba-rich phases increases as the T_g and the crystallization temperatures increase. The BS2 glasses with both the lowest T_g and lowest DSC crystallization temperatures show the most barium disilicate crystal. This leads to the conclusion that the metastable monoclinic high-$BaSi_2O_5$ is favored in these conditions. The small differences in glass synthesis conditions and chemicals used strongly influence the relative proportions of phases which crystallize and their kinetics. In-situ and ex-situ diffraction measurements confirm the conclusions above. The structural distinctions between the barium silicate crystals and the BS2 supercooled liquid, and the implications for the role of structural polymerization are discussed. We conclude that high-$BaSi_2O_5$ or $Ba_6Si_{10}O_{26}$ are the predominant phases in the earliest stages of crystallization. This study highlights the extreme sensitivity of BS2 glass crystallization kinetics and pathways to minor differences in composition and synthesis conditions and explains the different conclusions reached by distinct authors that worked on the crystallization of BS2 glasses.

1. Introduction

Barium disilicate ($BaO{\cdot}2SiO_2$) glass display a peculiar crystallization process when heat-treated; it nucleates in the sample interior as sub-100 Å spherulites, which are followed by axialite or composite spherulite growth, and finally sub-to euhedral crystals after recrystallization [1–3]. Early studies on barium silicate glass-ceramics drew particular attention as acicular morphologies doubled their flexural strength and significantly increased their elastic moduli [4]. Along with the high thermal expansion of crystalline barium silicates [5], these properties have made barium silicate-based glass-ceramics excellent candidates for solid-oxide fuel cell sealant materials [6]. Barium silicate glass-ceramics have also

* Corresponding author. Universidade Federal de São Carlos, Departamento de Física, Rod. Washington Luis, Km 235 13565-905, São Carlos, SP, Brazil.
E-mail address: benjamin.moulton@fau.de (B.J.A. Moulton).

https://doi.org/10.1016/j.ceramint.2022.11.277
Received 13 August 2022; Received in revised form 17 November 2022; Accepted 21 November 2022
Available online 24 November 2022

received renewed interest as potential fiber optic laser material [7], re-writable optical storage media [8] and, when doped with rare-earth elements, show impressive persistent phosphorescence over 10 h [9,10]. In addition to these important applications, the fact that barium silicate glasses show volume nucleation on the experimental timescale has made them the focus of considerable scientific investigations [11–18]. Although the stoichiometric $BaO{\cdot}2SiO_2$ composition (BS2) clearly shows *volume* nucleation, there is an ongoing discussion as to whether this constitutes a *homogeneous* versus *heterogeneous* case. We continue this debate below.

Within the $BaO–SiO_2$ system, the disilicate composition, $BaSi_2O_5$, is particularly interesting because a variety of structures are found that depart from several heuristic rules established for other simple binary silicates. For example, typically higher temperatures produce more symmetric structures whereas for barium disilicate the low temperature polymorph sanbornite has a higher symmetry (orthorhombic) than the monoclinic high-$BaSi_2O_5$ polymorph [19]. Unexpectedly the high--$BaSi_2O_5$ appears to form before the equilibrium phase, sanbornite, at large degrees of supercooling [1,20]. In part, this behavior was explained recently by Moulton et al. [20], as being due to the alternating orientation of tetrahedra in the high-temperature polymorph, which vary in orientation, as expected in the supercooled liquid structure, in contrast to the uniform orientation of tetrahedra in the sanbornite structure. This reconstructive phase change is clearly shown in thermograms in the presence of a second exothermic peak [20,21] and is accompanied by a coarsening of the crystals [1]. Recently, Takahashi and colleagues were the first to provide a definitive interpretation for the presence of high-$Ba_5Si_8O_{21}$ in the axialites in addition to epitaxial growth of high-$BaSi_2O_5$ [22,23]. This work was more profound as they identified the commonality among *volume* nucleating silicate glasses — all crystallize to 'low dimensional' structures [23].

In a multi-method study, Cai et al. [24], showed diffraction and atomic-scale resolution TEM nano photographs of axialites showing (sub-)regions containing Ba:O ratios pertaining to the $Ba_6Si_{10}O_{26}$ and $Ba_5Si_8O_{21}$ compositions. Ultimately, this study concluded that Ba-rich phases nucleate concurrently, if not before, a barium disilicate phase and, therefore, they inferred the process to be heterogeneous [24]. The presence of $Ba_6Si_{10}O_{26}$ found in several studies [20,24] is interesting as it is unstable and at equilibrium decomposes below 1300 °C [25],

$$Ba_6Si_{10}O_{26} \rightarrow BaSi_2O_5 + Ba_5Si_8O_{21} \quad (1)$$

The nucleating phase in BS2 glass, and whether it is a disilicate polymorph or a non-stoichiometric phase (e.g., high-$Ba_5Si_8O_{21}$), ultimately remains unclear. If the latter is true, one possible explanation is that the non-stoichiometry is related to liquid-liquid phase separation or a 'heterogeneous structure' within the barium disilicate liquid. Phase separation has been clearly observed in barium silicate glasses up to 28 mol. % BaO and may occur at slightly higher BaO contents but at quite low temperatures (<600 °C), where it is kinetically inhibited and easily avoided [26–28]. However, liquid-liquid phase separation does not take place in stoichiometric BS2 glass.

Furthermore, the diffusion coefficients of crystal growth decouple from those of viscosity somewhere between 785 °C and 870 °C [21], further emphasizing that structural changes occur in the supercooled liquid somewhat above the calorimetric glass transition temperature (T_g), at 690–700 °C when heated at a rate of 10 K/min. Importantly, in this range from 690 to 870 °C, the maximum steady state nucleation rate is found [12,14,29]. In fact, structural changes in the liquid were recently tracked during isothermal heat treatments of supercooled liquid $BaSi_2O_5$ at 790 °C using Raman spectroscopy [30]. Ultimately, polymerization ($SiO_2^0 \rightarrow SiO_{2.5}^{1-} + \frac{1}{2}O^{2-}$) producing some free oxygen, O^{2-}, was shown to precede the appearance of crystals within the supercooled liquid [30,31].

Another possible explanation for the multitude of crystal phases could be related to different treatment temperatures and to the fact that it is *practically impossible* to produce a perfectly stoichiometric $BaO{\cdot}2SiO_2$ glass. There is always some departure from ideal stoichiometry producing a glass that is slightly enriched or impoverished in barium and silica. Moreover, each glass batch produced at different laboratories always use distinct chemical reagents with different amounts and types of trace element impurities (OH^-, Sr, Ca, Al, etc.). Hence, all glasses are slightly different from each other. Finally, due to the substantial difference in the atomic mass of Ba and Si, and high melt viscosity, it is rather difficult to produce homogeneous glasses of this system. Along the years we have developed an experimental procedure to improve the melt homogeneity, which is not used by all research groups.

As a result of the ambiguity in the nucleating phase(s) and contradictory reports in the literature on the crystallization pathways of the BS2 glass, we have decided to compare the $BaSi_2O_5$ glasses made by three different groups and analyze them using *the same thermal treatment conditions and the same equipment* to determine whether or not they display a systematic crystallization behavior. In total, six barium disilicate glasses were produced at three separate labs and then characterized, heat treated, and analyzed at the Federal University of São Carlos. This research was conducted in two stages: First, the precursor disilicate glasses were characterized using DSC and Raman spectroscopy; second, another monolith from the same glass batch were heat treated at the maximum of the first DSC crystallization temperature (T_{p1}) and quenched immediately. These *treated samples* were then characterized by Raman spectroscopy and XRD. Additional monoliths from each batch were used to measure the glass density, and the same glass chip was used to measure the FTIR spectra to determine the OH^- content. The main differences in these six barium disilicate glasses were the precursor raw materials, number of times remelted, and the thermal treatment conditions.

This approach follows our initial study [20], however, that study was completed on a single glass batch. Therefore, it is unclear whether these

Table 1
Synthesis conditions of barium disilicate glasses.

ID	Synthesis Local	Calcination		Heating rate[a]	Initial Melting		# of times melted	Annealing	
		T °C	t h	° K/min	T °C	t h		**T °C**	**t h**
B1	UEPG	1350	36	10	1550	0.5	3	650	2
B2	UFSCar	1350	36	>20	1550	0.5	3	600	2
B3	UFSCar	none		>20	1550	0.5	3	n.a.[b]	
B4	UFRGS	1350	15	10 - 5 - 4	1550	3	1	600	3
B5	UEPG	1350	36	10	1550	0.5	3	650	2
B6[c]	UEPG	1350	36	10	1550	0.5	3	650	2

[a] Sample B2 and B3 were inserted into the hot furance estimating the rate as a minimum of 20 K/min; Sample B4 was heating at 10K/min until 1100 °C, 5 K/min until 1350 °C and 4 K/min until the melting point.
[b] n.a. = not applicable; the sample was not annealed.
[c] B7 was taken from the bottom of the crucible from the same batch as B6 which was taken from the central region.

initial results are representative of BS2 glasses in general. To generalize our findings, or not, we re-evaluate the glass used in Moulton et al. [20], and compare to the results of 5 new BS2 glasses. The synthesis conditions and sample nomenclature are reported in Table 1. Before discussing our results, we summarize more of the debate around nucleation in supercooled barium disilicate to provide a framework for the results below.

1.1. A condensed overview of crystallization in supercooled barium disilicate liquids

Early crystallization studies of barium disilicate liquid always found nuclei as <500 nm-sized spherulites (spherically symmetric crystal aggregates nucleating from a point source) [1,32]. With either increasing time or temperature these spherulites provide nucleation sites for larger spines, described as *axialites*, at the spherulite-melt interface. At increasingly long times, 1000 h at 700 °C, these spherulites coarsen and eventually recrystallize to a barium disilicate polymorph [1]. We emphasize that *spherulites* are aggregates of acicular crystals growing simultaneously outward in all directions and it should be highlighted that the spherulitic morphology is found over six orders of magnitude in scale from sub-micron [32] to up to a few meters [33,34]. There may be some orientational restriction but importantly, the aspect ratio of these acicular crystals is similar. In contrast, *axialites* are a composite crystal morphology which consist of a central *spine,* or trunk, described originally as a *midrib* [1], on which epitaxial growth of a fine *fibrillar* crystal aggregates occurs. In these examples, the axialite is an intermediate morphology between spherulitic and dendritic morphologies. This distinction is essential in evaluating which phase nucleates first, as these morphologies occur separately in phase space [2], as found in the classic work of Lofgren [35].

According to Lewis et al. [2], the evolution of crystal morphology with temperature and time of BS2 glass shows the transition in crystal morphologies with increasing temperature and time as the following: spherulites → composite spherulites (including axialites) → faceted crystals (coarse laths, euhedral grains). Lewis et al. [2] concluded that the diffuse diffraction profiles (SAED and XRD) of the nuclei did 'not permit an unambiguous identification' although these profiles are different from sanbornite and similar to the monoclinic structure with the α lattice parameter of 32.95 Å. The α lattice dimension is clearly indicative of the high-$Ba_5Si_8O_{21}$ phase, solved a year after Lewis's study along with the $Ba_4Si_6O_{16}$ and $Ba_6Si_{10}O_{26}$ phases [36]. Critically, in addition to high-$Ba_5Si_8O_{21}$ the absence of weaker reflections and pseudohexagonal axial pattern suggested that there may be another related monoclinic phase present as well [2]. In fact, most crystal phases in the $BaO–SiO_2$ system have monoclinic symmetry, including high-$BaSi_2O_5$. It is also likely that the low temperature polymorphs, low-$Ba_5Si_8O_{21}$ and low-$Ba_4Si_6O_{16}$, are also monoclinic, although their crystal structures have not been solved, despite appearing in the phase diagram [25]. In summary, the early studies concluded that the **nuclei are spherulitic with monoclinic symmetry,** possibly containing multiple phases whose diffraction patterns do not match that of sanbornite.

To complicate matters, these studies were followed by a select area electron diffraction (SAED) study which identified the spherulitic nuclei as monoclinic high-$BaSi_2O_5$ and the latter axialites as having a spine of sanbornite with a fibrillar overgrowth of high-$BaSi_2O_5$ [32]. This study did not report other monoclinic phases, richer in BaO. In a series of studies using powder-XRD and SAED, Takahashi et al. [37,38], provide evidence of high-$Ba_5Si_8O_{21}$ in the spine and high-$BaSi_2O_5$ in the fibrillar overgrowths of their axialites. They concluded that *homogeneous nucleation of $Ba_5Si_8O_{21}$ and high-$BaSi_2O_5$ occurs* due the low dimensionality of the structures [23]. More recently, Moulton et al. [20], showed that the broad diffraction profiles may obscure other Ba-rich phases such as $Ba_6Si_{10}O_{26}$, high-$Ba_5Si_8O_{21}$ and high-$Ba_4Si_6O_{16}$. The Moulton et al. study reported two important inferences: 1) the presence of Ba-rich phases is not related to minor discrepancies in major element composition as the features were found in both a practically stoichiometric BS2 glass as well as a glass with ~0.4 mol. % departure from the nominal stoichiometric composition; and, 2) the distribution in tetrahedral connectivity in barium disilicate liquid is abundant in $Q^{2\text{-}4}$ and in the same proportions as found in Ba-rich crystals, such as $Ba_5Si_8O_{21}$ or $Ba_6Si_{10}O_{26}$. Therefore, subregions within the liquid with the stoichiometry of Ba-rich phases may be expected [20].

Direct evidence for Ba-rich phases, including both $Ba_6Si_{10}O_{26}$ and $Ba_5Si_8O_{21}$, has been shown in high-resolution bright field TEM micrographs where subregions within a 'needle-like regions' have been reported [24,39]. Further heat treatment of these samples at 725 °C indicated peaks near −90 ppm in one dimensional ^{29}Si MAS NMR data and peaks at Q = 1–1.4 $Å^{-1}$ small-angle X-ray scattering (SAXS), both of which are signatures of a barium disilicate phase. Ultimately, this study relied on TEM results of the epitaxial overgrowths to infer that heterogeneous nucleation had taken place in the early crystallites. This conclusion is in doubt for two reasons. The first reason, is that by definition the axialites (needle-like crystals) nucleate heterogeneously, as discussed above [2,32]. Second, the authors recount that the TEM images are of the epitaxial overgrowths rather than on the trunks because they were unable to identify the phases due to amorphization of the samples. If Ba-rich phases were to have formed first they would have produced ^{29}Si NMR resonances at various frequencies between −80 and −82 ppm [40] due to the presence of Q^2 tetrahedra and also in the SAXS measurements. Ultimately, these studies make important observations regarding the nanoscale crystallization pathway in supercooled barium disilicate liquid [24,39].

Homogeneous nucleation occurs with equal probability in all volumes of a liquid, whereas heterogeneous nucleation is found when solid particles reduce the energy barrier required to form a critical nucleus preferentially promoting nucleation on the top of the catalyst [41]. In considering whether BS2 liquid nucleates heterogeneously or homogeneously [17,23,24,30], several questions arise:

- First, what is the nucleating phase? (If the high-$BaSi_2O_5$ disilicate polymorph nucleates, should this still be considered homogeneous nucleation?)
- Second, if the nucleating phase is a Ba-rich phase, what is the scale of these structural heterogeneities? Are similar structures found in the liquid (if so, then does this signify homogeneous nucleation?) or are they formed due to a catalyst (if so, then what is the catalyst)?
- Third, what are the practical consequences of these results?

Also, the effects of impurities and minor departures from stoichiometry on glass crystallization kinetics are not clearly known. Identifying these departures and the structural differences between the crystals and liquids is fundamental to this debate, as developed further below.

2. Methods

UFSCar glass preparation (Samples B2 and B3). The preparation of B2 and B3 glass samples used analytical grade reagents of barium carbonate (Sigma-Aldrich, ≥99%) and silica (Mineração Santa Rosa, Zetasil 2, 99,99%). B2 is the same sample as in our previous studies [20, 30]. The reagents were dried in a furnace for 12 h at 120 °C prior to use. The mixture B2 was homogenized and calcined in a platinum crucible for 36 h at 1350 °C and then melted at 1550 °C for 30 min. This "calcination" step was designed to form $BaSi_2O_5$ crystals, which were then melted. The B3 glass composition was prepared using the same reagents, but in this case the calcination step was not performed. B3 was melted directly at 1550 °C. Then, each liquid was quenched by pouring them onto a steel plate and re-melted three times to minimize the formation of bubbles and streaks and to improve the chemical homogeneity. In the last re-melting, the liquids were pressed between two stainless steel plates (splat-cooling). Both samples have had their

compositions measured by EPMA. The measurement conditions have been reported elsewhere [30], showing that they have molar BaO and SiO_2 contents of 33.5(±0.4) and 65.7(±0.3), and 33.4(±0.5) and 66.4 (±0.5) for B2 and B3, respectively. Both glasses contain minor (<0.18) of Na_2O and CaO and other impurities, <0.1 of SrO, K_2O and Al_2O_3.

UFRGS glass preparation (Sample B4). Barium disilicate glass ($BaO{\cdot}2SiO_2$) was prepared using barium carbonate ($BaCO_3$ - Sigma-Aldrich ≥99%), and silica (SiO_2), (Sigma-Aldrich, ≥99.9%). The B4 sample is that same as in our previous study [18]. The SiO_2 and $BaCO_3$ were dried in furnace for 4 h at 120 °C. After the reagents were weighed and mixed, the powders were calcined at 1350 °C for 15 h in a Pt crucible before being melted at 1550 °C for 3 h in an electric furnace. The melt was quenched on a steel plate, re-melted one additional time for 0.5 h at 1550 °C and finally quenched again on a steel plate. The sample was then annealed at 600 °C (~100 °C below the T_g) for 3 h and left to cool slowly to room temperature.

UEPG glass preparation (Samples B1, B5, B6). Three batches of BS2 glass, B1, B5 and B6, were melted according to Table 1. The glasses were prepared from a mixture of barium carbonate ($BaCO_3$ – 99%) and silica (SiO_2, 99.5% EMSR - Santa Rosa Zetasil 2) powders. The reagents were dried over a period of 12 h at 120 °C. After weighing, each batch was mixed in a roller mill for 12 h. The resulting powder was calcined at 1350 °C for 36 h in a platinum crucible in ambient (air) atmosphere in a Deltech electrical furnace to form $BaO{\cdot}2SiO_2$ crystals. The temperature was then raised to 1550 °C and held for 30 min until the batch was completely molten. The obtained melt was poured and pressed between two stainless steel plates. The material was remelted/cast three times for homogenization, and the obtained blocks of 45 × 20 × 3 mm^3 and cylinders measuring 40 mm in length x 12 mm in diameter were quickly placed in a furnace at 40 °C below the glass transition temperature (T_g ~690 °C) and cooled at 2 °C/min, to relieve the residual stresses.

Sample B1 was produced from a batch with $BaCO_3$ from Anidrol (>99%). Samples B5 and B6 were made using $BaCO_3$ from Dinâmica (99.98%), but in two different glass batches. Glass-ceramics samples derived from these samples have had their mechanical properties investigated [42]. In addition, a seventh BS2 glass sample, B7, was analyzed and was taken from the outer portion of the glass batch B6. That the samples were from the same batch was not known before the samples were treated and analyzed. The results, including DSC, Raman spectroscopy and X-ray diffraction, for the B6 and B7 are within error of one another indicating that the differences between glass batches *with different thermal histories and precursor materials* is much greater than the variation *within a single batch*. As a result, we will not discuss sample B7 further, as the analysis of B6 applies to B7. Evidently, the differences *between* batches are much greater than *within* any given batch.

Characterization and Analysis. Once synthesized, the six glasses were then characterized at UFSCar. The glass transition (T_g), the onset of crystallization (T_x), the crystallization (T_{p1}) and phase transition/recrystallization (T_{p2}) temperatures were determined using a differential scanning calorimeter (DSC) on a NETZSCH STA 449C thermal analyzer. Small cubes were cut from each glass batch to produce a ~40 mg sample used for each experiment. All experiments used a 10 °C/min heating rate, which was comparable with our previous studies [15,19]. Repeated measurements using the same conditions (e.g., sample mass, heating rate, etc.) of the B3 glass sample over a period of months indicated the reproducibility of the DSC peak temperatures is ±2 °C.

In a second step, a small piece of each glass batch (~40 mg) was heat treated in a tube furnace to the first crystallization temperature (T_{p1}) using a heating rate of 10 °C/min and quenched immediately in air. This procedure was used to determine which phases were involved in this early crystallization step. Note that surface crystallization under these conditions is negligible. All samples appeared somewhat cloudy white with varying degrees of opacity, presumably related to the crystal size and volume fraction. The samples heated up to T_{p1} constitute the **treated samples**.

The original untreated glasses as well as these treated samples were then investigated by Raman spectroscopy and subsequently powder X-ray diffraction (XRD) to determine the phases produced. Raman spectra were measured on the bulk sample, on both the exterior surfaces as well as on the interior surface of fractured monoliths. After the Raman experiments, the samples were then powdered and diffractograms were measured.

Raman spectra of bulk BS2 cubic monoliths were taken using 488 nm source at room temperature using an 1800 slits/mm grating, 100 μm confocal hole and an 100× objective. With ~15 mW on the sample, each spectrum took ~4 min and is the average of 36 individual spectra to give the reported spectra. The energy scale was calibrated both the laser line and main Si peak set to 520.7 cm^{-1}. As a measure of the reproducibility of these spectra two main peaks of low-$BaSi_2O_5$ spectrum were measured as having a frequency (FWHM) of 534.2 cm^{-1} (10.3) and 1076.4 cm^{-1} (4.7) which is within error from our previous study at 535.2 cm^{-1} (8.5) and 1076.8 cm^{-1} (4.6) [20]. Overall, these measurements have a precision ~1.0 cm^{-1} and a resolution <0.5 cm^{-1}.

Diffractograms of powdered barium disilicate were taken on a Rigaku Ultima IV diffractometer using a Cu Kα source (λ = 1.541 Å) in continuous scanning mode 0.05°/min in steps of 0.02° 2θ from 15 to 45°. This range was chosen to cover the characteristic diffraction peaks of the barium disilicate polymorphs, $Ba_6Si_{10}O_{26}$, $Ba_5Si_8O_{21}$, and $Ba_4Si_6O_{16}$ which represent the phases identified as possible within this system. Due to the possibility of crystal intergrowths and the poorly crystalline nature of the samples in general these results provide a guide to the process, however; convergence of attempted Rietveld refinements was not successful due to the breadth, scarcity, and superposition of the diffraction peaks.

Fourier Transform Infrared (FTIR) spectra were used to evaluate the water content of the BS2 glasses following Stolper [43] and Behrens [44]. The FTIR measures were conducted using a PerkinElmer Spectrum GX spectrometer operating in transmittance mode with a 4 cm^{-1} resolution in the 2000–4000 cm^{-1} range. Transmission spectra were taken from glass 'plates' polished to have parallel sides which were used for FTIR measurements only. We convert the FTIR data from transmittance (T%) to absorbance (A%) to facilitate calculations of glasses water (A = 2 - log (% T)) Accurate determination of the water content requires the density to be known. Therefore, the glasses densities were measured with analytical balance, Mettler Toledo AX204, with a precision of 0.0001 g by the immersion method in distilled water, using Archimedes' principle at 25 °C. The densities agree extremely well with published values [45], e.g., ~3.67 g/cm^3. Density (ρ) of samples was obtained employing the relation (1) as given below:

$$\rho = \frac{m_d}{m_{st} - m_{im}} \rho_{water} \tag{2}$$

where, ρ is the sample density, m_d is the sample dry weight, m_{st} is the weight of the saturated sample, m_{im} is the weight of the sample immersed in water and ρ_{water} is the water density. As the glass samples are non-porous, the dry and saturated weights were considered equal.

In-situ high-temperature synchrotron XRD experiments (λ_0 = 1.2398 Å) were made at the XPD beamline [46] of LNLS in Campinas, Brazil. High resolution (0.004°) diffractograms were continuously recorded between 10 and 33° 2θ on a Mythen detector (~3 min/pattern) while the B3 glass was powdered and held in a spinning sample holder. Diffraction patterns are the averaged diffractograms taken in 3.5° 2θ windows and show temperature window of 6 °C/spectrum as the sample was heated up to 1000 °C. Temperature precision is ±10 °C based on measurements of cubic MgO as a standard, however, the accuracy should be better, ~6 °C, comparable to the resolution of the measurements.

3. Results and discussion

The BS2 glass batches have been numbered according to their

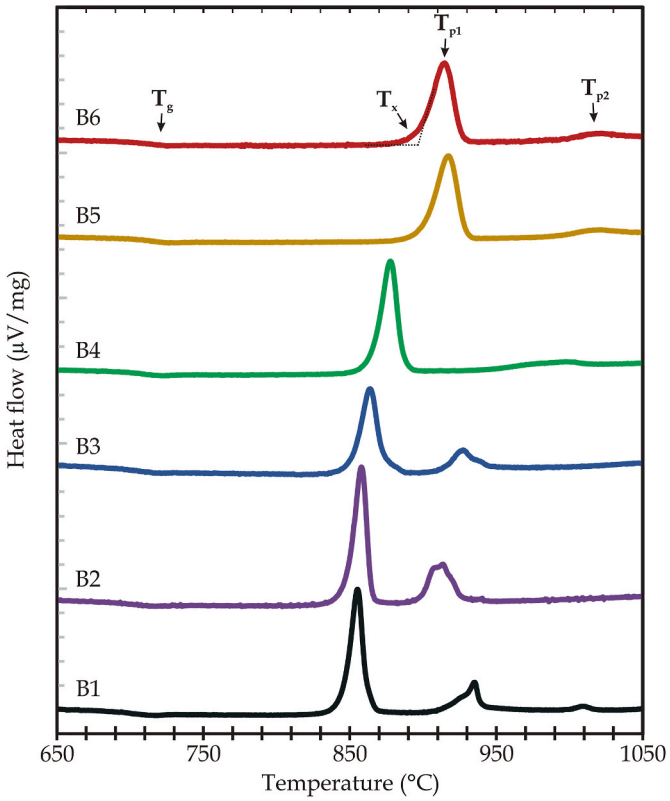

Fig. 1. DSC traces for untreated barium disilicate glass monoliths. Values are reported in Table 3.

increasing glass transition temperatures, T_g, and their first crystallization peak temperatures, T_{p1} (Fig. 1). B1 has the lowest T_{p1} and three exothermic events (Table 3). Samples B2–B4 having low T_{p1} and only two exothermic events whereas samples B5–B6 which have a higher T_{p1} and a broad, weak T_{p2} recrystallization event. The glass compositions have been determined by electron probe microanalyzer (EPMA), see Table 2.

Sample B2 is the same glass studied by Moulton et al. [20], and B4 is the same glass studied by Evaristo et al. [18], and their thermograms, diffractograms, and Raman spectra agree with those previously reported. The conclusions of these studies were incomplete and are refined below.

3.1. Analysis of calorimetric results

DSC traces for six BS2 glasses shows that samples B1–B4 glasses have T_g at 690 °C ± 4° whereas the T_g of the glasses B5 and B6 are near 700 °C (Table 3). Glass B1 displays three exothermal events at T_{p1}-T_{p3} at 855, 935 and 1009 °C. The B2 and B3 glasses have similar behaviors with the onset of crystallization temperatures (T_x), T_{p1} and T_{p2} of 849 (±2°), 861 (±3°) and 921 °C (±7°), respectively. That T_{p2} is lower here than in sample B1 is important. T_x and T_{p1} for the B4 glass systematically increased by 14 °C relative to B2/B3. Glasses B5 and B6 have considerably higher temperature T_x and T_{p1} at 897 and 915 °C, respectively, and T_{p2} is broad and centered at 1022 °C. Although sample B4 has a first crystallization temperature near B2 and B3, its second event, T_{p2}, is at 997 °C, closer to glasses B5 and B6. Therefore, B4 may be considered as a glass with an intermediate between B3 and B5.

Table 3
Temperatures (°C) of thermal events.

ID	T_g	T_x	T_{P1}	T_{P2}
B1[a]	689	845	855	935
B2	690	847	858	914
B3	686	851	864	928
B4	692	865	878	997
B5	702	897	917	1022
B6	700	896	915	1022

[a] Sample B4 has a third exothermic peak at 1009 °C.

The third exothermic event in sample B1 is notable. A third thermal event at temperatures between 1070 and 1180 °C was observed by Ramsden and James (1984) and inferred to be due to the precipitation of cristobalite. It is not clear whether the third event in sample B1 is comparable or not, but it is unlikely due to the presence of cristobalite, as the composition is enriched slightly in Na_2O, at the expense of SiO_2 (Table 2). This fact argues against the interpretation that cristobalite forms due to phase separation, as inferred by Ramsden and James. However, they might have studied a hypo-stoichiometric glass. Either way, sample B1 displays a depressed T_{p1} and delayed T_{p2}, which differs from the remaining samples.

3.2. Raman spectra of starting glasses

The Raman spectra of the starting glasses are all close to that of published $BaSi_2O_5$ glass spectra [20,47] and therefore the subtle differences become important (Fig. 2). Glasses B2 and B3 do not have appreciably different spectral envelopes. B1 and B5 show a small peak near 860 cm^{-1} (see arrow in Fig. 2) indicative of the formation of Si–O stretching modes associated with Q^1 tetrahedra [40,47]. The B1 glass also has a slightly more intense 935 cm^{-1} peak, indicating that it has more Q^2 units. The features of B1, Q^1 and increased Q^2, indicate that this sample is enriched somewhat in modifier oxides relative to the other compositions, as reported in its chemistry (Table 2). Glasses B1, B5 and B6 also display a slight positive shift in the O–Si–O bending mode 'doublet', at 550-600 cm^{-1}, where the local maximum of this doublet shifts from 545 to 555 cm^{-1} from B3 to B6, respectively. There are other minor changes at lower frequencies, but these are difficult to discern with confidence due to the sensitivity of the filters close to the laser line. In summary, with the exception of B1 and B5 the remaining glasses display typical BS2 glass spectra with slight modifications most obvious in the bending mode doublet.

Table 2
Density and chemistry of barium disilicate glasses.

ID	n[a]	BaO	SiO_2	Al_2O_3	Na_2O	CaO	SrO	OH-	Density[b]
		mol. %						ppm	g/cm^3
B1	5	33.4(1)	65.9(1)	0.1(0)	0.5(1)	b.d.	b.d.	77	3.719
B2	12	33.5(4)	65.7(3)	0.1	0.2(1)	0.1(2)	n.a.	98	3.692
B3	18	33.4(6)	66.4(6)	b.d.	0.2(0)	b.d.	b.d.	95	3.665
B4	5	32.1(6)	67.1(5)	0.3(0)	0.4(2)	b.d.	b.d.	94	3.677
B5	5	31.6(2)	67.3(1)	0.5(0)	0.4(1)	b.d.	0.1(0)	70	3.655
B6	10	31.4(1)	67.4(2)	0.4(0)	0.6(1)	0.1(0)	0.1(0)	66	3.652

[a] n is the number of EMPA analysis per sample. B.d. is below detection limit. N.a. is not analyzed.
[b] Estimated standard deviation is ±0.002.

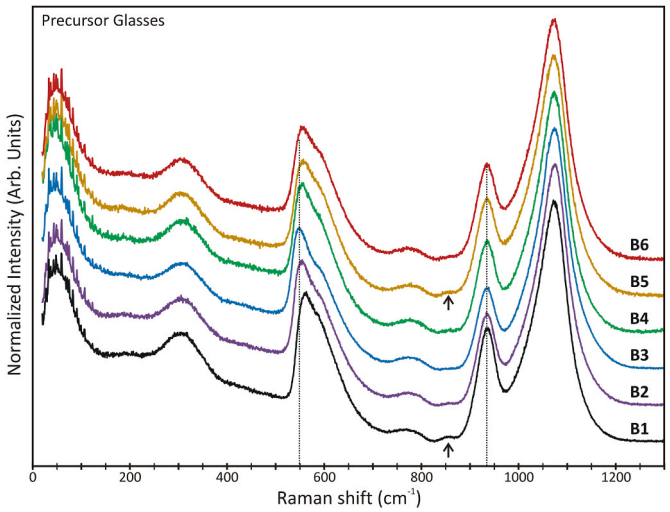

Fig. 2. Background corrected Raman spectra of glassy barium disilicate. Intensities have been normalized to the 1070 cm^{-1} peak. Spectra have been offset vertically for comparison. Spikey peaks <200 cm^{-1} on top of the boson peak are due to scattering from air.

3.3. Diffraction results

The diffractograms of the treated samples show poorly-crystalline glass-ceramics (Fig. 3). The Sample B1 shows a strong shoulder at 22.3° that is indicative of the [310] or [011] planes of high- or low-$BaSi_2O_5$, respectively. The breadth of this feature obscures the distinction between the disilicate polymorphs. The diffractogram of B1 shows a prominent peak at 23.6° and multiple peaks between 27.0 and 30.0°. The shoulders at 23.6 and 27° are indicative of Ba-rich phases and are best explained by the presence of $Ba_6Si_{10}O_{26}$, though $Ba_5Si_8O_{21}$ may also be present. The shoulder between 28 and 30° in the diffractogram of B1 is best attributed to high-$BaSi_2O_5$. Sample B1, is therefore best explained as a combination of high-$BaSi_2O_5$ and $Ba_6Si_{10}O_{26}$, though sanbornite and $Ba_5Si_8O_{21}$ may be present.

B2 and B3 display either an intense peak or shoulder at 22.3°, indicating that a $BaSi_2O_5$ polymorph is a dominant phase. The shoulder from 22.5 to 24.0° and the broad feature between 27.0 and 30.0° likewise indicate the presence of a Ba-rich phase and confirm that the high-$BaSi_2O_5$ polymorph is present in B2 and B3. In sample B4, the shoulders centered at 23.3 and 27.7° 2θ indicate that this sample contains more of the non-stoichiometric phases than samples B2 and B3. Taken together, these observations indicate that high-$BaSi_2O_5$ is the dominant phase present with lesser amounts of $Ba_6Si_{10}O_{26}$ in the B2 and B3 monoliths, though again, sanbornite and $Ba_5Si_8O_{21}$ may be present in lesser proportions.

The samples, B5 and B6, display a slightly asymmetric peak centered at 23.0° – essentially at the midpoint between the main peaks of the $BaSi_2O_5$ polymorphs and $Ba_6Si_{10}O_{26}$. The diffraction is weaker, and the peaks are broader in diffractograms of these samples, indicating that the crystallinity is lower than in the other samples. Nonetheless, the prominent feature at 23.0° suggests a mixture of $BaSi_2O_5$ and $Ba_6Si_{10}O_{26}$ are present. Though this interpretation should be treated with more caution than for the other samples. Overall, the diffraction profile of these samples appears to be somewhat 'intermediate' between B1 and B2 in that its peaks do not coincide precisely with either those of a disilicate polymorph or a more Ba-rich phase.

In summary, as T_{p1} decreases in the from sample B2 to B6 the diffraction intensity and peak sharpness increase as does the 22.3° feature indicating that one of the $BaSi_2O_5$ polymorphs is found at lower crystallization temperatures. The broad feature between 28.0 and 30.0° indicates that high-$BaSi_2O_5$ is the dominant polymorph though sanbornite cannot be entirely eliminated. The shoulder at 22.5–24.0° clearly indicates the presence of at least one non-stoichiometric phase that is best explained by $Ba_6Si_{10}O_{26}$ though $Ba_5Si_8O_{21}$ should not be excluded. The sample B1 does not fit these trends as its T_{p1} is the lowest but the diffraction peaks associated with the non-stoichiometric phases are more intense than those associated with a disilicate phase.

3.4. Raman spectra of heat-treated samples

The peaks in the Raman spectra are considerably broadened relative to crystalline standards (Fig. 4). The main features in these spectra are

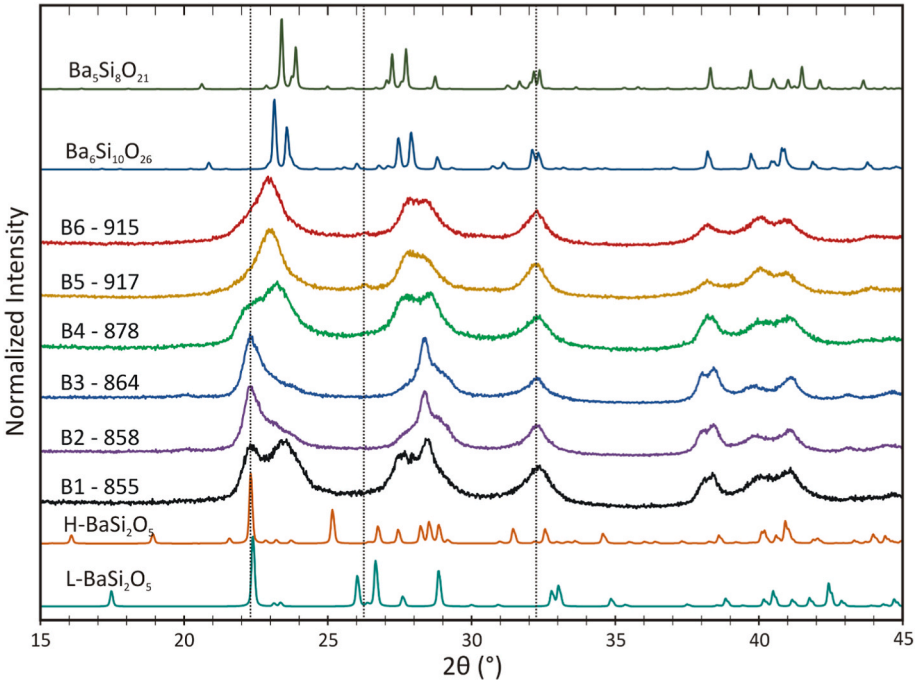

Fig. 3. Diffractograms for heat treated barium disilicate samples and standards.

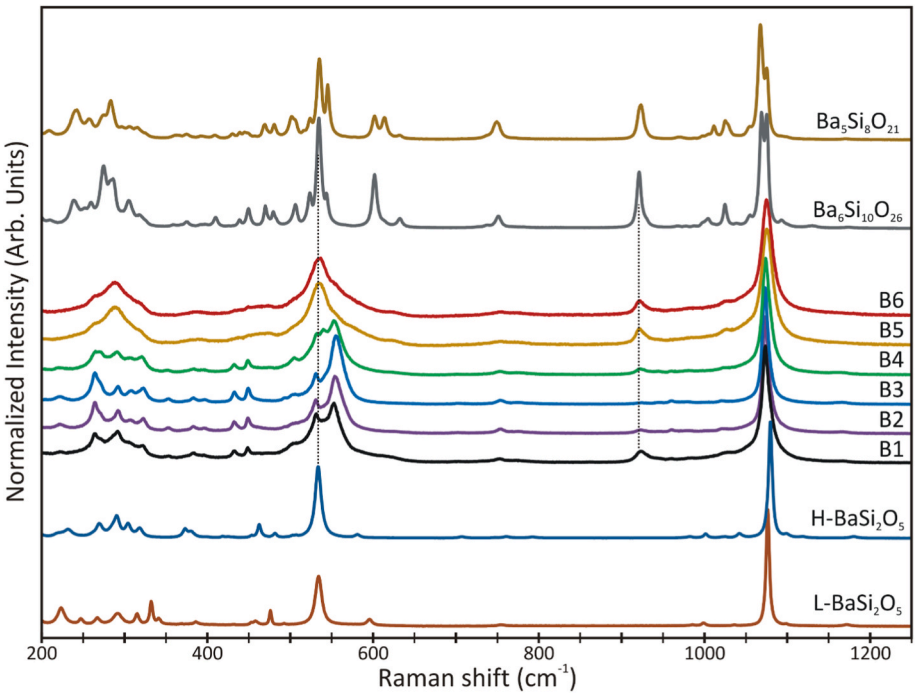

Fig. 4. Background corrected Raman spectra of BS2 glass-ceramics heated to T_{p1}. The high frequency region is the focus of Fig. 5A below.

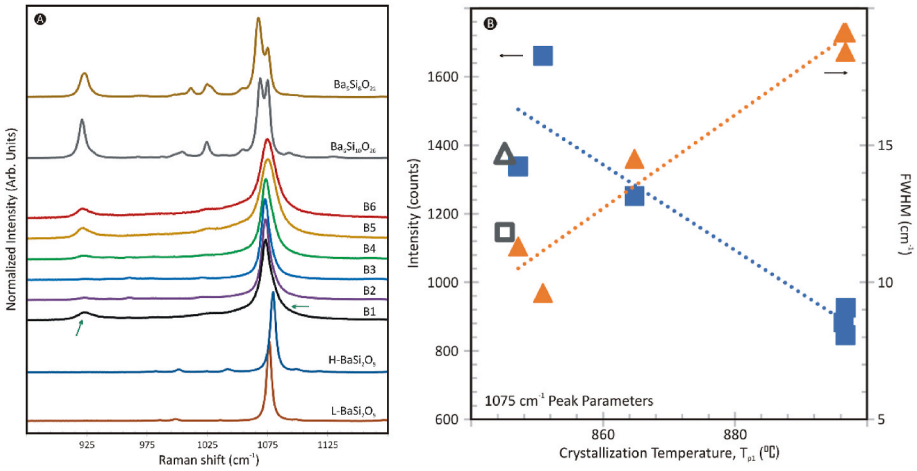

Fig. 5. A) High frequency region of the Raman spectra of the treated samples. B) Intensity (squares) and full-width at half-maximum (FWHM, triangles) plotted versus T_{p1} temperature (Table 2). Grey symbols (color online) come from B1 whereas B2–B3 and B4–B6 values are plotted together and follow clear trends. Values for the peak parameters are reported in Table 4. Error bars are smaller than the symbols. (For interpretation of the references to color in this figure legend, the reader is referred to the Web version of this article.)

threefold: a triple-pointed feature spanning 250-350 cm^{-1}, the broad 'doublet' feature between 500 and 600 cm^{-1}, and the most intense band near ~1070 cm^{-1}. The first two features, <700 cm^{-1}, are related to external bending/deformation modes where the low frequency modes usually have a strong influence of Ba cations whereas the latter modes at 500-600 cm^{-1} come from Si–O–Si, O–Si–O and to a lesser degree Si–O–Ba motions [40,48]. The third high-frequency feature near 1070 cm^{-1} is associated with stretching modes of individual Si–O bonds [40, 48]. A partial fit yields the peak parameters of the three spectral features reported in Table 4.

Table 4
Peak fit parameters determined from partial fits of Raman spectra for treated samples[a].

ID	T_{P1}	250–350 Modes						500–600 Modes				900–1100 Modes				
		Center	FWHM	Center	FWHM	Center	FWHM	Center	FWHM	Center	FWHM	Center	FWHM	Center	FWHM	Intensity
B1	845	**265**	**18.0**	**292**	24.4	318	15.0	**530**	26.0	553	26.2	926	**17.2**	**1074**	**14.7**	**1146**
B2	847	**265**	**11.7**	**293**	23.8	322	9.7	**530**	19.3	556	19.6	927	23.6	**1074**	**11.3**	**1338**
B3	851	**266**	**12.3**	**292**	12.7	318	18.6	**531**	19.8	556	17.1	n.d.		**1074**	**9.6**	**1660**
B4	865	**267**	**17.0**	**292**	27.9	319	13.9	536	36.1	555	20.9	928	29.4	**1074**	**14.5**	**1251**
B5	897	267	33.9	290	24.0	**310**	17.0	534	30.6	567	**57.2**	924	**15.7**	1075	19.1	925
B6	896	267	30.7	290	24.3	**311**	16.4	534	29.8	561	**56.5**	924	**16.7**	1075	19.1	882
B7	897	267	30.6	289	24.0	**309**	17.1	534	30.4	563	**54.9**	924	**15.2**	1075	18.4	845

[a] Center and FWHM of Lorentzian lineshapes are given in wavenumbers and intensity given in absolute counts. N.d. is not determined. Highlights indicate distinctions noted in text.

In all spectra the first feature, the triplet-like feature centered around 300 cm^{-1} (Fig. 4), displays one of two patterns. The first pattern is identified by the multiple well-defined peaks where the most intense peak is found close to 260 cm^{-1}, for example in the B2 spectrum, whereas the second pattern is identified by a broad triplet which is most intense in the middle near 290 cm^{-1}, as in the B6 spectrum. The former pattern is broadly similar to that of high-$BaSi_2O_5$ whereas the latter pattern, particularly the relative peak intensities, are reminiscent of $Ba_6Si_{10}O_{26}$ [20,40]. The samples B1–B4, all display the high-$BaSi_2O_5$--like pattern whereas the B5 and B6 samples display the pattern more closely resembling $Ba_6Si_{10}O_{26}$.

A similar division between glasses B1 to B4 versus B5 and B6 may be made based on the doublet feature found from 500 to 600 cm^{-1}. The Raman spectra of B1 to B4 display a clear 'doublet' with local maxima near 535 and 555 cm^{-1}. The spectra of B5/B6 display a more symmetric distribution of peaks which are centered near 535 cm^{-1}. The 535-peak (s) is not diagnostic, as all of the barium silicate phases discussed here have intense bending modes within a few wavenumbers of this frequency and the vibrational origin of these modes are unique [20,40,48]. Weak peaks near 600 and 750 cm^{-1} are all better explained by the presence of either $Ba_6Si_{10}O_{26}$ or $Ba_5Si_8O_{21}$. The sharpness of the doublet feature reflects the overall crystallinity of the treated samples. However, these peaks are not diagnostic of the crystal phases. The 555-peak is more ambiguous in origin and therefore will be omitted from further discussion.

The final region of the spectra is the high frequency region where the vibrational modes originate from the stretching of specific Si–O bonds [40,48]. There are two key features in this region (Fig. 5), a weak band at 925 cm^{-1} and the intense mode found around 1075 cm^{-1} which originate from the Q^2 and Q^3 sites, respectively [40,48]. Notably, only the Ba-rich phases, $Ba_6Si_{10}O_{26}$, $Ba_5Si_8O_{21}$, and $Ba_4Si_6O_{16}$, contain Q^2 sites whereas all of these phases, including the $BaSi_2O_5$ polymorphs, contain Q^3 site(s). Therefore, the presence of the 925-peak is unequivocal evidence for the presence of the Ba-rich phases. The spectra of the B1, B5 and B6 samples have notably sharp peak near 925 cm^{-1} indicating the presence of Ba-rich phase(s) (Fig. 5A; Table 4). This is consistent with the diffraction data above and indicates that $Ba_6Si_{10}O_{26}$ is present in these samples.

At room temperature, the intense Q^3 mode of high-$BaSi_2O_5$ is found at higher frequency, 1079 cm^{-1}, than that of sanbornite at 1077 cm^{-1} [20]. In the Ba-rich phases, $Ba_4Si_6O_{16}$, $Ba_5Si_8O_{21}$ and $Ba_6Si_{10}O_{26}$, the main Q^3 modes monotonically shift to higher frequencies with increasing Ba content, from 1061 to 1069 cm^{-1} [49]. Table 4 shows that in all spectra of the treated samples this peak is found at 1074 cm^{-1} in samples B1–B4 or at 1075 cm^{-1} in B5 and B6. As with the diffraction peaks at ~23.0° above, the frequency of the Q^3 mode (1075 cm^{-1}) is between that of the $BaSi_2O_5$ polymorphs (1077-1079 cm^{-1}) and $Ba_6Si_{10}O_{26}$ (1069 cm^{-1}). A shift of 1 cm^{-1} between samples B1–B4 and B5–B6 may not appear significant, however, it is when the other peak parameters are considered. Fig. 5B shows the measured counts and full-width at half-the-maximum (FWHM) of the Q^3 peak for the treated samples. The +1 cm^{-1} shift is accompanied by a significant decrease in intensity and systematic increase in the FWHM of this peak which increases from 9 to 15 cm^{-1} in the B1–B4 spectra to 19 cm^{-1} for the B5–B6 spectra. For the ideal crystal the FWHM of this peak is 4–6 cm^{-1} depending on the phase [20,40,48]. Using the FWHM of this peak as an indicator of degree of crystallinity suggests that the samples are more crystalline as B3>B2>B4>B1*>B5/6. Thus, sample B1, although it has the lowest T_{p1}, has a bandwidth, 17.2 cm^{-1}, that is comparable to samples B5–B7, ranging 15.2–16.7 cm^{-1}, and a band intensity of 1146 cts which lies between samples B4 and B5, at 900–1250 cts. The width and intensity are much higher and lower, respectively, than in the B2 and B3 samples (Table 4). These differences are entirely consistent in the enhanced signals from Ba-rich phases as evidenced by the 925 band in the Raman spectrum (Fig. 5a) and the intense peak at 23.6° in its diffraction profile (Fig. 3). Moreover, these effects may be further understood by the slightly higher modifier (Na_2O + BaO) content of this glass (Table 2). The sodium may diffuse faster than the larger barium cations, depressing the initial thermal events, while delaying the recrystallization, as the much smaller Na^+ cations are not well suited to the sanbornite structure. These results highlight the sensitivity of Raman spectroscopy to identify and distinguish the crystallization process, even in complex cases.

If B1 is excluded, the remaining B2–B6 samples display a monotonic relationship with increasing intensity and decreasing FWHM as the first crystallization temperature, T_{p1}, decreases (Fig. 5B). This behavior follows the complementary thermogram (Fig. 1) and diffractogram (Fig. 3) results which show that lower crystallization temperatures and lower phase transition temperatures, T_{p2}, are associated with more barium disilicate phase. Based on the evidence above, we conclude that it is the high-$BaSi_2O_5$ polymorph that forms first, although some $Ba_6Si_{10}O_{26}$ likely forms simultaneously. That being said, we cannot eliminate with certainty the presence of sanbornite or $Ba_5Si_8O_{21}$, though arguments can be made based on the topology of the former (uniform orientation of the tetrahedra) and instability of the latter (its composition is furthest from the disilicate composition and may form through decomposition, via reaction (1)) why they are less likely to form than high-$BaSi_2O_5$ and $Ba_6Si_{10}O_{26}$. This interpretation is in agreement with the evidence presented by Moulton et al. [20] and Cai et al., [24]. Ultimately, the above systematic trends strongly suggest that high-$BaSi_2O_5$ is the preferred nucleating phase.

3.5. Density and water content

Using the Lambert-Beer law [43,44], the water content of these glasses is $C_{water} = 1802 \times A_{2800}/(d\rho\varepsilon)$, where A_{2800} is the absorbance (peak height) of the 2800 cm^{-1} band, d is the thickness of the sample in centimeters, ρ is the density in g/L (Table 2), ε is the molar absorption coefficient in L mol^{-1} cm^{-1}. The value of ε was taken as 56 L mol^{-1} cm^{-1} based on previous results of hydrous BS2 glasses [44]. The FTIR spectra (Fig. 6) yield H_2O contents between 66 and 98 ppm (Table 2). Though we note that H_2O reflects the total hydrous content, i.e., no distinction is made between OH^- and H_2O species. In general, the water content increases with decreasing T_{p1} temperature, however, the ~50 ppm difference in overall contents cannot explain the dramatic shifts in the crystallization peak temperatures displayed above. This is inferred from comparing the differences between B2, B3 and B4 which have OH^- contents of 98, 95 and 94 ppm, but show T_{P1} temperatures increasing

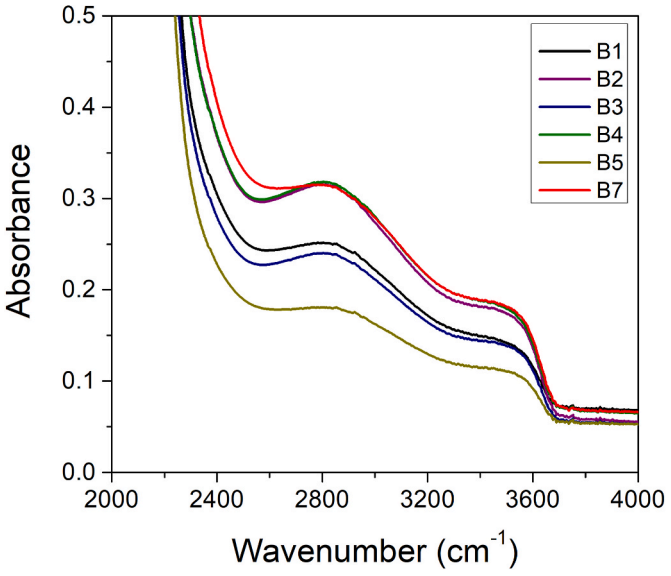

Fig. 6. Mid IR spectra of the water bands in barium disilicate glasses. Note spectra have not been normalized to the sample thickness.

from 858 to 864–878 °C, respectively. Clearly, the subtle differences in water content do not correlate to the crystallization temperatures as no systematic behavior is discerned. Likewise, B1 has the lowest T_{p1} and the lowest water content, 66 ppm, the opposite of the general trend of the data. Thus, it seems that the influence of 50–100 ppm of water is overridden by the overall compositional differences of the six glasses.

3.6. Consequences of stoichiometry

Several questions were raised regarding the nucleation process in BS2 glasses. Now we endeavour to provide some answers. First, we observed a trend where samples with the lowest T_g, first (T_{p1}) and second (T_{p2}) crystallization temperatures show features in both Raman spectra and diffractograms that indicate higher concentrations of high-$BaSi_2O_5$ and a higher degree of crystallinity. However, evidence for at least one Ba-rich phase is always also found. The features indicative of the Ba-rich phase are best explained by the presence of the unstable phase $Ba_6Si_{10}O_{26}$. The presence of $Ba_5Si_8O_{21}$ is not excluded by our data, however, whether it is actually present or whether it forms from the breakdown of $Ba_6Si_{10}O_{26}$ is not possible to discern. The evidence presented by Cai et al. [24], suggest that subregions of disilicate crystals contain this stoichiometry, which is consistent with the studies of crystalline barium silicates, which show that these phases readily form intergrowths of various barium silicate stoichiometries to the point that even substructures of unknown phases, such as $Ba_7Si_{12}O_{31}$ or $Ba_8Si_{14}O_{36}$, are possible [50].

To understand why these phases routinely appear in the crystal products derived from barium disilicate glass, and are much less common in other systems, one needs to understand the structural building blocks which relate the barium silicate phases from the disilicate to the metasilicate composition. The general formula for this barium silicate series is $Ba_{m+1}Si_{2m}O_{5m+1}$, where crystal phases are known for m = 1, 3, 4, 5, and ∞ corresponding to the crystalline phases $Ba_2Si_2O_6$, $Ba_4Si_6O_{16}$, $Ba_5Si_8O_{21}$, $Ba_6Si_{10}O_{26}$ and the $BaSi_2O_5$ polymorphs, respectively [36]. Therefore, all of these phases can be built by the addition of 1 mol of BaO to multiples of the $BaSi_2O_5$ component. For example,

$$Ba_6Si_{10}O_{26} \leftrightarrow 5BaSi_2O_5 + BaO \quad (3)$$

$$Ba_5Si_8O_{21} \leftrightarrow 4BaSi_2O_5 + BaO \quad (4)$$

and so on … The difference between these phases is in how many moles of barium disilicate are formed as fluctuations in the liquid density of plus or minus a single Ba and O are readily achieved without a significant energy barrier [14,39,47,51]. Recent molecular dynamics simulations have shown that average Ba coordination by oxygen is 7.0–7.7 depending on the cut-off distance used, but with a wide distribution from 4 to 10 [47,51]. This average is somewhat lower than found in the barium silicate crystals discussed above, all of which have barium-oxygen coordination numbers between 8 and 9 [40], but highlights that a significant fraction of Ba^{2+} cations will be found having CN comparable to that found in the crystalline phases. This has been noted by Zanotto et al., as being an important factor promoting homogeneous nucleation [52]. As oxygen is ubiquitous, and only minimal adjustment to the local barium environments are needed, then perhaps the tetrahedral part of the liquid network may provide insight.

Moulton et al., have recently pursued an in-depth study on the tetrahedral network of the glass forming region in the BaO–SiO_2 system using Raman, ^{29}Si MAS and static NMR spectroscopies as well as molecular dynamics simulations [47,53]. Their polymerization model determined that BS2 glass has 14, 72 and 15 ± 3% of Q^2, Q^3 and Q^4 units, respectively [47]. Note that this conclusion was based on quantitative agreement between all spectroscopic techniques. This is of note as large discrepancies in the proportions of the Q^n species in BS2 glasses with values of Q^3 varying by up to ~30% in the absolute concentration (i.e., an uncertainty of ~40% of the measured concentration) depending on the details of the analysis. This included several physically implausible Q^n distributions.

Where Q^4 is present, as all models show for glass or liquid $BaSi_2O_5$, they must suffer depolymerization, via $Q^4 + \frac{1}{2}O \rightarrow Q^3$, to be used in any of these crystal structures. Likewise, all Q^2 must be polymerized via $Q^2 - \frac{1}{2}O \rightarrow Q^3$, to be used in the sanbornite or high-$BaSi_2O_5$. During crystallization of supercooled liquid $BaSi_2O_5$ both reactions occur in proportion such that $Q^2 + Q^4 \rightarrow 2Q^3$, or in stoichiometric terms including barium: $SiO_3^{2-} + SiO_2^0 + Ba^{2+} \rightarrow BaSi_2O_5$. This has been directly observed using Raman spectroscopy [30].

In BS2 glass, the Q^3 species constitute the majority at ~70% and the Q^2 to Q^3 proportions is ~1:5, if the Q^4 species are excluded. In contrast in the barium disilicate polymorphs contain only Q^3 units whereas $Ba_4Si_6O_{16}$, $Ba_5Si_8O_{21}$, and $Ba_6Si_{10}O_{26}$, contain both Q^2 and Q^3 and have Q^2:Q^3 ratios of 1:2, 1:3 and 1:4, respectively (e.g., see Refs. [40,48] for discussion). Therefore, the undercooled liquid structure will have a modified random network containing connectivities most closely resembling the structures of $Ba_6Si_{10}O_{26}$ and the $BaSi_2O_5$ polymorphs. Given that the probability of dynamically heterogeneous regions within the liquid structure where all of the tetrahedra share a unified orientation, as found in sanbornite, is likely both spatially and temporally limited, then it may be expected that the tetrahedra are randomly oriented. This distribution in tetrahedral orientations bares more similarity to the high-$BaSi_2O_5$ structure and explains why this may be the preferred nucleating phase even if it well out of equilibrium, as we have argued [20]. If not for the high-$BaSi_2O_5$ polymorph it may be expected that the nucleation rates would be considerably depressed.

In the end, a couple critiques regarding the nucleation of BS2 liquids are warranted. According to Kelton and Greer [41] *homogeneous* nucleation may occur with equal probability in any part of the system, whereas *heterogeneous* nucleation occurs when or where a catalyst reduces the work of nucleation producing highly probable nucleation sites. Given that there is some distribution of structural units present in the glass or liquid, which are not present in the crystalline phases, implies that not all regions within the liquid are capable of forming nuclei. Therefore, one could argue that barium disilicates do display heterogeneous nucleation. However, by this definition essentially all silicate liquids, and perhaps all oxide liquids, would be precluded from discussions of homogeneous nucleation as all of them would exemplify heterogeneous nucleation. The liquid structures have a dynamic average where interconversion reactions between structural units are constantly ongoing and are only frozen in the glassy state. A more nuanced definition of heterogeneous nucleation may therefore be more practical. We suggest that heterogeneous nucleation may be restricted to situations where a catalyst is *known to be present*, for example by the presence of solid particles (and not by intrinsic dynamic heterogeneities), then the BS2 liquid may be considered a homogeneous nucleating system, as no crystal structures appear which are not innately possible in the liquid. In other words, as long as a metastable phase forms with equal probability in all regions of the SCL, this process should still be described as homogeneous nucleation.

A similar phenomenon has been reported for hypo- and hyper-stoichiometric lithium disilicate (LS2) glasses in which lithium-rich crystals (lithium metasilicate) form in the early stages of crystallization together with the stable phase LS2 [54]. Although in the case of $Li_2Si_2O_5$ liquids, no spatial association between phases was reported, unlike for $BaSi_2O_5$ liquids. From this perspective, both the BS2 and LS2 liquids can be rationalized without the resorting to the argument that they are heterogeneously nucleating liquids. In any case, the further departed the crystal composition (e.g., metasilicate crystals forming in a disilicate liquid) the less probable, or more time is required to observe, the formation of such phases. The paucity of observations in silicate liquids then becomes a consequence of the fact that there are only approximately a dozen stoichiometric silicate systems that are intrinsically inferred to nucleate homogeneously. Of these homogeneously

nucleating silicate systems, only a few compositions have received comprehensive attention of probes which are sufficiently sensitive enough to reveal the presence of minor phases, especially during the early stages of crystallization.

In summary, small deviations in bulk chemistry do not explain the presence of multiple barium silicate phases found, however, they may influence the relative proportions of the phases produced. Given the absence of trace element data, we cannot exclude the importance of dopants, however, five separate studies [1,20,24,55], including this one, have now documented the appearance of Ba-rich phases in the crystallization process of barium disilicate glasses. The appearance of LS in LS2 liquids stems from a similar phenomenon. This investigation leads to two conclusions: First, that minor deviations from ideal chemistry are unlikely to produce dramatic changes in nucleation rates, as would be the case if any of the dozens of minor impurities caused heterogeneous nucleation in the barium or lithium disilicate studies of different authors using distinct glass batches. Second, that non-stoichiometric phases precipitate due to the similarities between the liquid and crystal structures on the local and intermediate range scales. In other words, supercooled glass-forming liquids have static and dynamic heterogeneities with regions that resemble the structures of certain Ba-rich phases.

3.7. Final proof of the crystallization pathway

As a further confirmation of the intimate relationship between these phases, a series of heat treatments of these glasses were undertaken to confirm both the definitive presence and meta-stability of $Ba_6Si_{10}O_{26}$. Although only 1% of $Ba_6Si_{10}O_{26}$ was previously confirmed [20], here in a two-step treatment sample B5 underwent a nucleation step of 90 min at 700 °C and then coarsened for 12 h at 940 °C to produce a mixture of 39% $Ba_6Si_{10}O_{26}$ and 61% high-$BaSi_2O_5$ [42] (Fig. 7). This confirms the presence of these two phases, without necessity for other Ba-rich phases, and provides a unique solution to the diffraction pattern. This result indicates that it may be possible stabilizing and engineering non-stoichiometric phases for specific applications depending on the glass composition, source chemicals, and thermal treatment.

As final proof of the crystallization pathway, *in situ* high-temperature synchrotron XRD experiments were made at the XPD beamline [46]. High resolution (0.004°) diffractograms were recorded every 4 min while the powdered B3 sample was continuously heated up to 1000 °C. Fig. 8 shows a sharp change in pattern between the broad amorphous halo of the supercooled liquid $BaSi_2O_5$ and the distinctly crystalline peaks at 760 °C. At 760 °C, it takes longer than 30 min to induce surface nucleation in BS2 glass monoliths [56] and therefore, although the

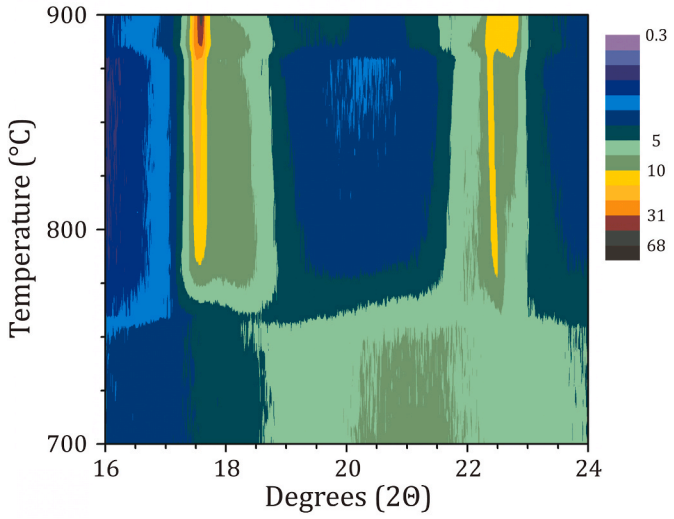

Fig. 8. In-situ high-temperature diffractogram heatmap showing crystallization of supercooled liquid $BaSi_2O_5$ between 700 and 900 °C. Color intensity scale is non-linear with values expressed as a percentage of the maximum counts attained in the fully crystalline sample. (For interpretation of the references to color in this figure legend, the reader is referred to the Web version of this article.)

sample is powdered we assert that the diffraction peaks predominantly come from the volume nucleation, at least at such early stages in the crystallization process. This interpretation is reinforced by >300 Raman measurements reported in our initial study [20], as well as from unpublished measurements of the glass surface, freshly cracked interior and multiple cross-section profiles of multiple BS2 glass monoliths. In all of the Raman spectra, whether surface or interior, the same progression as reported above is observed; poorly crystalline samples show broader and poorly resolved peaks, whereas longer heat treatments show the disappearance of the doublet between 530 and 550 cm^{-1}, and progressively sharpening of modes towards the characteristic lineshapes of sanbornite.

Note that the diffractograms presented in Fig. 8 are comparable to those in Fig. 3 when the source wavelengths and temperature are considered. At this wavelength the main diffraction peak of high-$BaSi_2O_5$ is found at $2\theta = 17.5°$ and the shoulder extends up to almost 19.0°. The diffractogram shows the initial crystallization from the supercooled liquid at 760 °C, where both the 17.5° and the shoulder

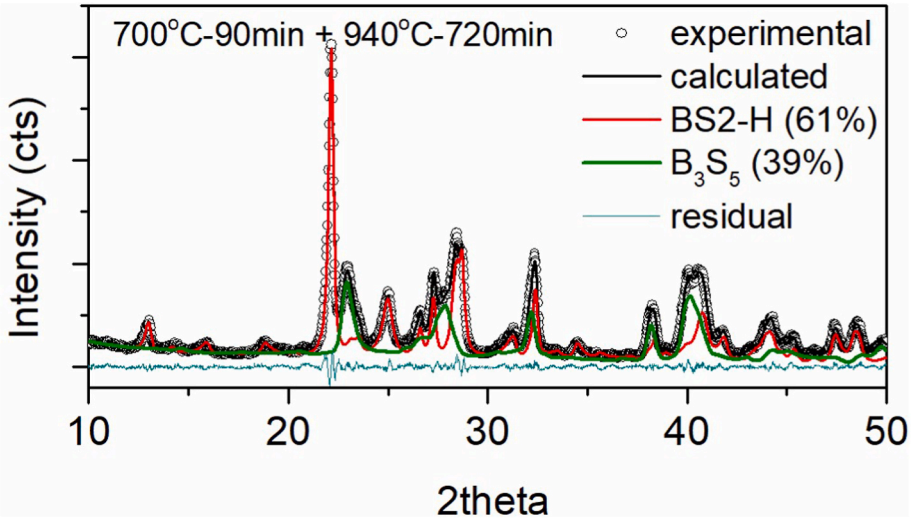

Fig. 7. Rietveld refinement of fully crystalized B5 sample showing successful refinement of 39% $Ba_6Si_{10}O_{26}$ (B_3S_5) and 61% high-$BaSi_2O_5$ (H-BS2).

feature appear simultaneously. The shoulder is best explained by the presence of $Ba_6Si_{10}O_{26}$, as shown in Fig. 7. By 875 °C, near the maximum DSC crystallization temperature, the intensity of the high-$BaSi_2O_5$ peak at 17.5° increases exponentially from 10% to 50%, and an intense shoulder develops at 22.6°. Overall, the diffraction peaks are too broad and Rietveld refinement was unsuccessful, however, the diffraction profiles between 760 and 870 °C are consistent with a mixture of high-$BaSi_2O_5$ and $Ba_6Si_{10}O_{26}$. Therefore, we conclude that these in-situ high-temperature XRD results reveal evidence for the simultaneous appearance of both high-$BaSi_2O_5$ and $Ba_6Si_{10}O_{26}$ forming as the initial nuclei.

4. Summary and conclusions

In comparing six (nominally) barium disilicate glasses, produced independently in three laboratories, using different precursor chemicals and synthesis conditions, we found the following trend between DSC exothermic events and crystallization products: As the first and second calorimetric crystallization temperatures decrease, the structural signals of a barium disilicate increase, indicating that a $BaSi_2O_5$ polymorph is strongly favored. Our X-ray diffraction and Raman evidence is best explained by (metastable, monoclinic) high-$BaSi_2O_5$, although no sample in this study, nor in previous studies, shows that this phase forms alone [1,20,24,39,57]. Here we provide direct evidence that **high-$BaSi_2O_5$ forms *simultaneously* with $Ba_6Si_{10}O_{26}$** early on the crystallization pathway. A similar phenomenon has been reported for lithium disilicate glasses in which lithium-rich crystals form in the early stages of crystallization together with the stable phase $Li_2Si_2O_5$ [54].

Heat treatments of these barium disilicate glasses did yield a sample that crystallized to a 40:60 mixture of $Ba_6Si_{10}O_{26}$ and high-$BaSi_2O_5$, thus, other phases are not necessary to explain our results. Taken together with the conclusions of previous studies [39,50], the initial nuclei which form in supercooled barium disilicate liquids likely have intergrowth- or defect-rich structures which are trapped during quenching and may be controlled by careful thermal treatment.

The relationship between structural fluctuations or dynamic heterogeneities and depolymerization of supercooled silicate liquids above the glass transition temperature remains an important issue to be investigated. Here direct evaluation of the Ba coordination and connectivity of the tetrahedral network were explored and highlight the similarities in the local environments of Ba and Q^n distribution with the crystal structures of $Ba_6Si_{10}O_{26}$ and high-$BaSi_2O_5$. We explain in detail why sanbornite is unlikely to be the nucleating phase – because all tetrahedra within the structure are pointing in the same direction. Therefore, high-$BaSi_2O_5$ may be energetically more favourable because it contains tetrahedra pointing in opposite directions, as expected of tetrahedra within a modified random network. In fact, the distribution of Q^2 and Q^3 species within the $BaSi_2O_5$ liquid have proportions close (~1:5) to that found in $Ba_6Si_{10}O_{26}$ (1:4). This is thought to explain the numerous reports of different non-stoichiometric phases in crystallization studies of stoichiometric barium silicate liquids, in contrast to other compositions where the relatively rare mixed connectivities phases, e.g., $Ba_6Si_{10}O_{26}$ or $Ba_5Si_8O_{21}$, are not stable. Ultimately, the presence of non-stoichiometric phases (relative to the composition under investigation), which appear in the binary BaO–SiO_2 phase diagram, or the presence of phases which are not shown to affect the nucleation rates, should not be considered as evidence of heterogeneous nucleation.

Finally, this exploratory study, using barium disilicate glasses as an example, highlights the extreme sensitivity of glass crystallization to composition, liquid structure, and synthesis conditions. The subtle differences in composition and thermal treatments explain why it is often difficult to reproduce crystallization experiments and reproduce glass-ceramics when one of the starting conditions is changed. Overall, these results also explain the often-reported discrepancies of different research groups that worked on this particular system.

Declaration of competing interest

The authors declare that they have no known competing financial interests or personal relationships that could have appeared to influence the work reported in this paper.

Acknowledgements

BJAM thanks the São Paulo Research Foundation (FAPESP) for research funding through grant no. 2016/18567-5. We greatly appreciate the support of CNPq and CAPES support to PSP, LDS and SRFS. LLE and SB thank CNPq (no. 406916/2016-0), the Rio Grande do Sul Research Foundation (FAPERGS) (19/2551-0001978-5), and CAPES (no. 1807654). FCS thanks CNPq (no. 311801/2017-0) and is grateful to C-LABMU/UEPG for the use of their experimental facilities. This research used resources of the Brazilian Synchrotron Light Laboratory (LNLS), an open national facility operated by the Brazilian Centre for Research in Energy and Materials (CNPEM) for the Brazilian Ministry for Science, Technology, Innovations and Communications (MCTIC). We thank M Montazerian, RS Silvo, MVS Rezende, and their students as well as the beamline staff for their support during our beamtime (proposal no. 20180393). FAPESP funding of the CEPID project (no. 2013/07793-6) is greatly appreciated. We thank the reviewer for helping to improve this contribution.

References

[1] M.H. Lewis, G. Smith, G. Smith, Spherulitic growth and recrystallization in barium silicate glasses, J. Mater. Sci. 11 (11) (1976) 2015–2026, https://doi.org/10.1007/PL00020327.
[2] M.H. Lewis, J. Metcalf-Johansen, P.S. Bell, Crystallization mechanisms in glass-ceramics, J. Am. Ceram. Soc. 62 (5–6) (1979) 278–288.
[3] S.W. Freiman, G.Y. Onoda, A.G. Pincus, Controlled spherulitic crystallization in $3BaO\text{-}5SiO_2$ glass, J. Am. Ceram. Soc. 55 (7) (1972) 354–359, https://doi.org/10.1111/j.1151-2916.1972.tb11309.x.
[4] S.W. Freiman, G.Y. Onoda, A.G. Pincusi, Mechanical properties of $3BaO.5SiO_2$ glass-ceramics, J. Am. Ceram. Soc. 57 (1) (1974) 8–12, https://doi.org/10.1111/j.1151-2916.1974.tb11352.x.
[5] L.A. Gorelova, R.S. Bubnova, S.V. Krivovichev, M.G. Krzhizhanovskaya, S. K. Filatov, Thermal expansion and structural complexity of Ba silicates with tetrahedrally coordinated Si atoms, J. Solid State Chem. 235 (2016) 76–84, https://doi.org/10.1016/j.jssc.2015.12.012.
[6] R. Trejo, E. Lara-Curzio, A. Shyam, M.J. Kirkham, V. Garcia-Negron, Y. Wang, Physical and mechanical properties of barium alkali silicate glasses for SOFC sealing applications, Int. J. Appl. Glass Sci. 3 (4) (2012) 369–379, https://doi.org/10.1111/ijag.12004.
[7] P. Dragic, C. Kucera, J. Furtick, J. Guerrier, T. Hawkins, J. Ballato, Brillouin spectroscopy of a novel baria-doped silica glass optical fiber, Opt Express 21 (9) (2013), 10924, https://doi.org/10.1364/OE.21.010924.
[8] S. Lin, H. Lin, Q. Huang, et al., A photostimulated $BaSi_2O_5:Eu^{2+}$,Nd^{3+} phosphor-in-glass for erasable-rewritable optical storage medium, Laser Photon. Rev. 13 (4) (2019), 1900006, https://doi.org/10.1002/lpor.201900006.
[9] P. Wang, X. Xu, D. Zhou, X. Yu, J. Qiu, Sunlight activated long-lasting luminescence from $Ba_5Si_8O_{21}:Eu^{2+},Dy^{3+}$ phosphor, Inorg. Chem. 54 (4) (2015) 1690–1697, https://doi.org/10.1021/ic5026312.
[10] Y. Jia, W. Sun, R. Pang, et al., Sunlight activated new long persistent luminescence phosphor $BaSiO_3:Eu^{2+}$,$Nd^{3}+$,Tm^{3+}: optical properties and mechanism, Mater. Des. 90 (2016) 218–224, https://doi.org/10.1016/j.matdes.2015.10.130.
[11] V.M. Fokin, A. Cabral Aluísio, R.M.C.V. Reis, M.L.F. Nascimento, E.D. Zanotto, Critical assessment of DTA-DSC methods for the study of nucleation kinetics in glasses, J. Non-Cryst. Solids 356 (6–8) (2010) 358–367, https://doi.org/10.1016/j.jnoncrysol.2009.11.038.
[12] V.M. Fokin, E.D. Zanotto, J.W.P. Schmelzer, Homogeneous nucleation versus glass transition temperature of silicate glasses, J. Non-Cryst. Solids 321 (1–2) (2003) 52–65, https://doi.org/10.1016/s0022-3093(03)00089-9.
[13] V.M. Fokin, A.S. Abyzov, E.D. Zanotto, D.R. Cassar, A.M. Rodrigues, J.W. P. Schmelzer, Crystal nucleation in glass-forming liquids: variation of the size of the "structural units" with temperature, J. Non-Cryst. Solids 447 (2016) 35–44, https://doi.org/10.1016/j.jnoncrysol.2016.05.017.
[14] A.M. Rodrigues, J.P. Rino, P.S. Pizani, E.D. Zanotto, Structural and dynamic properties of vitreous and crystalline barium disilicate: molecular dynamics simulation and Raman scattering experiments, J. Phys. D Appl. Phys. 49 (43) (2016), 435301, https://doi.org/10.1088/0022-3727/49/43/435301.
[15] A.M. Rodrigues, D.R. Cassar, V.M. Fokin, E.D. Zanotto, Crystal growth and viscous flow in barium disilicate glass, J. Non-Cryst. Solids 479 (October) (2018) 55–61, https://doi.org/10.1016/j.jnoncrysol.2017.10.007.

[16] J. Deubener, Structural aspects of volume nucleation in silicate glasses, J. Non-Cryst. Solids 351 (18) (2005) 1500–1511, https://doi.org/10.1016/j.jnoncrysol.2004.04.028.

[17] E.D. Zanotto, P.F. James, Experimental test of the general theory of transformation kinetics: homogeneous nucleation in a $BaO{\cdot}2SiO_2$ glass, J. Non-Cryst. Solids 104 (1) (1988) 70–72, https://doi.org/10.1016/0022-3093(88)90183-4.

[18] L.L. Evaristo, B.J.A. Moulton, P.S. Pizani, S. Buchner, Effect of high pressure on the structure of barium disilicate glass-ceramics, J. Non-Cryst. Solids 550 (August) (2020), 120380, https://doi.org/10.1016/j.jnoncrysol.2020.120380.

[19] K.F. Hesse, F. Liebau, Crystal chemistry of silica-rich Barium silicates III: refinement of the crystal structures of the layer silicates Ba2[Si4O10] (I), (Sanbornite), and Ba2[Si4O10] (h), Zeitschrift fur Krist - New Cryst Struct. 153 (1–2) (1980) 33–41, https://doi.org/10.1524/zkri.1980.0004.

[20] B.J.A. Moulton, A.M. Rodrigues, D.V. Sampaio, et al., The origin of the unusual DSC peaks of supercooled barium disilicate liquid, CrystEngComm 21 (17) (2019) 2768–2778, https://doi.org/10.1039/c8ce02054j.

[21] A.M. Rodrigues, D.R. Cassar, V.M. Fokin, E.D. Zanotto, Crystal growth and viscous flow in barium disilicate glass, J. Non-Cryst. Solids 479 (July 2017) (2018) 55–61, https://doi.org/10.1016/j.jnoncrysol.2017.10.007.

[22] Y. Takahashi, M. Osada, H. Masai, T. Fujiwara, Transmission electron microscopy and in situ Raman studies of glassy sanbornite: an insight into nucleation trend and its relation to structural variation, J. Appl. Phys. 108 (6) (2010), 63507, https://doi.org/10.1063/1.3487473.

[23] Y. Takahashi, H. Masai, T. Fujiwara, Nucleation tendency and crystallizing phase in silicate glasses: a structural aspect, Appl. Phys. Lett. 95 (2009), 071904, https://doi.org/10.1063/1.3206931.

[24] L. Cai, R.E. Youngman, D.E. Baker, et al., Nucleation and early stage crystallization in barium disilicate glass, J. Non-Cryst. Solids 548 (July) (2020), 120330, https://doi.org/10.1016/j.jnoncrysol.2020.120330.

[25] G. Oehlschlegel, Crystallization of glasses in the system $BaO{*}2SiO_2$-$2BaO{*}3SiO_2$, J. Am. Ceram. Soc. 58 (3–4) (1975) 148–149, https://doi.org/10.1111/j.1151-2916.1975.tb19584.x.

[26] P. Hudon, D.R. Baker, The nature of phase separation in binary oxide melts and glasses. I. Silicate systems, J. Non-Cryst. Solids 303 (3) (2002) 299–345, https://doi.org/10.1016/S0022-3093(02)01043-8.

[27] T.P. Seward, D.R. Uhlmann, D. Turnbull, Phase separation in the system BaO-SiO_2, J. Am. Ceram. Soc. 51 (5) (1968) 278–285, https://doi.org/10.1111/j.1151-2916.1968.tb13858.x.

[28] Y. Gueguen, P. Houizot, F. Célarié, et al., Structure and viscosity of phase-separated BaO-SiO_2 glasses, J. Am. Ceram. Soc. 100 (5) (2017) 1982–1993, https://doi.org/10.1111/jace.14642.

[29] A.M. Rodrigues, Processos difusionais, Cristalizacao e escoamento Viscoso em dissilicato de Bario vitreo, Federal University of Sao Carlos, 2014.

[30] B.J.A. Moulton, A.M. Rodrigues, P.S. Pizani, D.V. Sampaio, E.D. Zanotto, A Raman investigation of the structural evolution of supercooled liquid barium disilicate during crystallization, Int. J. Appl. Glass Sci. 9 (4) (2018) 510–517, https://doi.org/10.1111/ijag.12356.

[31] H.W. Nesbitt, G.M. Bancroft, G.S. Henderson, Polymerization during melting of ortho- and meta-silicates: effects on Q species stability, heats of fusion, and redox state of mid-ocean range basalts (MORBs), Am. Mineral. 105 (5) (2020) 716–726, https://doi.org/10.2138/am-2020-6841.

[32] A.H. Ramsden, P.F. James, The effects of amorphous phase separation on crystal nucleation kinetics in BaO-SiO_2 glasses - Part 2 Isothermal heat treatments at 700° C, J. Mater. Sci. 19 (9) (1984) 2894–2908, https://doi.org/10.1007/BF01026965.

[33] E. Bustos, W.A. Báez, L. Bardelli, et al., Genesis of megaspherulites in el viejo rhyolitic coulee (pleistocene), southern puna, Argentina, Bull. Volcanol. 82 (6) (2020), https://doi.org/10.1007/s00445-020-01382-8.

[34] C. Breitkreuz, J. Götze, A. Weißmantel, Mineralogical and geochemical investigation of megaspherulites from Argentina, Germany, and the USA, Bull. Volcanol. 83 (3) (2021) 14, https://doi.org/10.1007/s00445-021-01434-7.

[35] G. Lofgren, An experimental study of plagioclase crystal morphology; isothermal crystallization, Am. J. Sci. 274 (3) (1974) 243–273, https://doi.org/10.2475/ajs.274.3.243.

[36] K.F. Hesse, F. Liebau, Crystal chemistry of silica-rich Barium silicates I: refinement of the crystal structures of Ba4[Si6O16], Ba5[Si8O21] and Ba6[Si10O26], silicates with triple, quadruple and quintuple chains, Zeitschrift fur Krist - New Cryst Struct. 153 (1–2) (1980) 3–17, https://doi.org/10.1524/zkri.1980.0002.

[37] Y. Takahashi, M. Osada, H. Masai, T. Fujiwara, Crystallization and nanometric heterogeneity in glass: in situ observation of the boson peak during crystallization, Phys. Rev. B Condens. Matter 79 (21) (2009), 214204, https://doi.org/10.1103/PhysRevB.79.214204.

[38] Y. Takahashi, H. Masai, M. Osada, R. Ihara, T. Fujiwara, Formation of spherulite and metastable phase in stoichiometric $Ba_2Si_3O_8$ glass, J Ceram Soc Japan 118 (1382) (2010) 955–958, https://doi.org/10.2109/jcersj2.118.955.

[39] M.E. McKenzie, B. Deng, D.C. van Hoesen, et al., Nucleation pathways in barium silicate glasses, Sci. Rep. 11 (1) (2021) 15, https://doi.org/10.1038/s41598-020-79749-2.

[40] B.J.A. Moulton, E.O. Gomes, T.R. Cunha, et al., A theoretical and experimental investigation of hetero- versus homo connectivity in barium silicates, Am. Mineral. (2022), https://doi.org/10.2138/am-2021-7910.

[41] A.L. Greer, K.F. Kelton, Nucleation in Condensed Matter, Elsevier, New York, 2010.

[42] R.F. Sabino S do, B.G.B. Cordeiro, L.D. Silva, A.G.M. Pukasiewicz, E.D. Zanotto, F. C. Serbena, Microstructural and residual stress effects on toughening of stoichiometric $BaO.2SiO_2$ glass-ceramics, J. Eur. Ceram. Soc. 42 (13) (2022) 6119–6134, https://doi.org/10.1016/j.jeurceramsoc.2022.05.073.

[43] E. Stolper, Water in silicate glasses: an infrared spectroscopic study, Contrib. Mineral. Petrol. 81 (1) (1982) 1–17, https://doi.org/10.1007/BF00371154.

[44] H. Behrens, R. Kappes, P. Heitjans, Proton conduction in glass - an impedance and infrared spectroscopic study on hydrous $BaSi_2O_5$ glass, J. Non-Cryst. Solids 306 (3) (2002) 271–281, https://doi.org/10.1016/S0022-3093(02)01190-0.

[45] N.P. Bansal, R.H. Doremus, Handbook of Glass Properties, Academic Press, New York, 1986.

[46] F.F. Ferreira, E. Granado, W. Carvalho Jr., S.W. Kycia, D. Bruno, R. Droppa Jr., X-ray powder diffraction beamline at D10B of LNLS: application to the Ba_2FeReO_6 double perovskite, J. Synchrotron Radiat. 13 (1) (2006) 46–53, https://doi.org/10.1107/S0909049505039208.

[47] B.J.A. Moulton, A. Picinin, L.D. Silva, et al., A critical evaluation of barium silicate glass network polymerization, J. Non-Cryst. Solids 583 (February) (2022), 121477, https://doi.org/10.1016/j.jnoncrysol.2022.121477.

[48] E.O. Gomes, B.J.A. Moulton, T.R. Cunha, L. Gracia, P.S. Pizani, J. Andrés, Identifying and explaining vibrational modes of sanbornite (low-$BaSi_2O_5$) and $Ba_5Si_8O_{21}$: a joint experimental and theoretical study, Spectrochim. Acta Part A Mol Biomol Spectrosc 248 (2021), 119130, https://doi.org/10.1016/j.saa.2020.119130.

[49] A.G. Santos, B.J.A. Moulton, A.A. Cabral, Discoveries about the structure of alkaline earth-bearing borosilicate glasses doped with TiO_2 revealed by Raman spectroscopy, J. Non-Cryst. Solids 578 (September 2021) (2022), 121349, https://doi.org/10.1016/j.jnoncrysol.2021.121349.

[50] M. Czank, P.R. Buseck, Crystal chemistry of silica-rich barium silicates, Z. für Kristallogr. - Cryst. Mater. 153 (1–2) (1980) 19–32, https://doi.org/10.1524/zkri.1980.0003.

[51] M. Rai, G. Mountjoy, Molecular dynamics modelling of the structure of barium silicate glasses BaO–SiO_2, J. Non-Cryst. Solids 401 (2014) 159–163, https://doi.org/10.1016/j.jnoncrysol.2013.12.026.

[52] E.D. Zanotto, J.E. Tsuchida, J.F. Schneider, H. Eckert, Thirty-year quest for structure-nucleation relationships in oxide glasses, Int. Mater. Rev. 60 (7) (2015) 376–391, https://doi.org/10.1080/09506608.2015.1114706.

[53] B.J.A. Moulton, L.D. Silva, C. Doerenkamp, et al., Speciation and polymerization in a barium silicate glass: evidence from ^{29}Si NMR and Raman spectroscopies, Chem. Geol. 586 (2021), 120611, https://doi.org/10.1016/j.chemgeo.2021.120611.

[54] P. Soares, E. Zanotto, V. Fokin, H. Jain, TEM and XRD study of early crystallization of lithium disilicate glasses, J. Non-Cryst. Solids 331 (1–3) (2003) 217–227, https://doi.org/10.1016/j.jnoncrysol.2003.08.075.

[55] Y. Takahashi, H. Masai, T. Fujiwara, Nucleation tendency and crystallizing phase in silicate glasses: a structural aspect, Appl. Phys. Lett. 95 (7) (2009) 1–4, https://doi.org/10.1063/1.3206931.

[56] A.M. Rodrigues, D.R. Cassar, V.M. Fokin, E.D. Zanotto, Crystal growth and viscous flow in barium disilicate glass, J. Non-Cryst. Solids 479 (October 2017) (2018) 55–61, https://doi.org/10.1016/j.jnoncrysol.2017.10.007.

[57] Y. Takahashi, M. Osada, H. Masai, T. Fujiwara, Structural heterogeneity and homogeneous nucleation of $1BaO$-$2SiO_2$ glass, Appl. Phys. Lett. 94 (21) (2009), 211907, https://doi.org/10.1063/1.3142394.